JOURNAL OF GEOPHYSICAL RESEARCH, VOL. 95, NO. B2, PAGES 1343–1358, FEBRUARY 10, 1990

Color and Albedo of the South Polar Layered Deposits on Mars

KEN E. HERKENHOFF AND BRUCE C. MURRAY

Division of Geological and Planetary Sciences, California Institute of Technology, Pasadena

Five color/albedo units, including polar frost, have been recognized and mapped in the southern layered deposits on Mars. Atmospheric dust scattering was measured in shadows and modeled in order to remove the component of brightness in Mars images due to the atmosphere and quantify the albedo and color of the surface. The layered deposits appear to be mantled by red dust, except where eolian stripping has exposed the underlying bedrock. Frost and bare ground are mixed below the resolution of the images in many areas adjacent to the polar cap, some of which appear to be younger than the surrounding layered terrain. Dark material has been deposited in topographic depressions in much of the south polar region, including the layered deposits. The available observational data suggest that the layered deposits are composed of bright dust, ice, and a small amount of dark material. If the dark material is sand, a periodic change in polar winds seems required in order to transport the sand poleward into the layered terrain. In any case, the observations are not consistent with the layered deposits being composed only of bright dust and ice. The Mars observer camera and infrared instruments should be particularly useful in this investigation.

1. INTRODUCTION

The polar layered deposits on Mars probably record climate variations over at least the last 10^7–10^8 years [*Murray et al.*, 1972; *Carr*, 1982; *Plaut et al.*, 1988]. The composition, stratigraphy, and morphology of these layered deposits must be understood to determine the processes responsible for their formation and erosion and hence the mechanisms by which climatic variations are recorded. A common presumption among Mars researchers is that the layering somehow reflects variations in the proportions of dust and ice deposited during many climate cycles [*Toon et al.*, 1980; *Cutts et al.*, 1979; *Squyres*, 1979; *Howard*, 1978; *Cutts*, 1973]. The purpose of this paper is to use photometric measurements of the surface brightness and color of the layered deposits to constrain their composition and texture and hence their origin.

Howard et al. [1982] studied the geology of the north polar layered deposits, and *Thomas and Weitz* [1989] analyzed their color and albedo by using high-resolution Viking Orbiter images. Comparable studies of the south polar region have been limited by the lower resolution of the Viking imaging data. The striking contrasts in size, setting, and appearance of the north and south polar layered deposits suggest significant differences in their formation and evolution. Further photometric and morphologic study of the south and comparison of the two regions may offer insights into Mars' climate history over the last 10^8 years or more.

Viking Orbiter 2 imaged the south polar region in three colors, typically at a resolution of a few hundred meters per pixel. In this paper we first describe how these color data were processed and then discuss the effects of atmospheric scattering on the apparent surface brightnesses. We modeled the dust scattering in shadows and used the results to estimate the atmospheric component of brightness in the images (details of the method are presented in the Appendix). The dust-scattering properties found in our analysis are similar to those found in previous studies. Removal of the atmospheric effects from the color images then allows estimation of surface reflectance and permits five color/albedo surface units to be quantified within the south polar layered terrain. The color and albedo of these mapped units are then interpreted in terms of composition and texture. Finally, we consider several hypotheses of the composition of the layered deposits and discuss the implications for their formation.

Paper number 89JB01429.
0148-0227/90/89JB-01429$05.00

2. PROCESSING AND MAPPING METHODS

T. Becker (U.S. Geological Survey, Flagstaff, Arizona) used Viking Orbiter 2 images of the south polar region taken through three different filters (violet, green, and red) to construct the digital color mosaic shown in Plate 1. The 18 images (six in each of three colors) in the mosaic were taken nearly simultaneously during orbit 407 (L_s = 341°), at phase angles around 85°. The incidence (solar zenith) angle varies from about 60° at the top of the mosaic to 85° at the bottom. The south pole is at bottom center, near the lower edge of the residual cap.

The images were radiometrically calibrated in Flagstaff using the Planetary Image Cartography System (PICS), so that the data value in each pixel represents the actual reflectance (I/F) observed. The relative calibration error measured where the images overlap is as large as 10%, so that the absolute uncertainty in calibration is no less than 10%. This result is consistent with the 13% (1σ) absolute uncertainty near midscale in the Viking television calibration reported by *Klaasen et al.* [1977]. No estimates of the radiometric accuracy of PICS have been published, and the absolute uncertainty of the Viking Orbiter calibration may be greater than 13%. Preliminary analysis of Viking Orbiter 1 Phobos images shows differences of up to 18%, but discussion of these data is beyond the scope of this paper. In the absence of precise knowledge of the absolute radiometric uncertainty in the Viking data used here, we will use the 13% absolute uncertainty given by *Klaasen et al.* [1977] in the discussions that follow.

Because the green filter band pass (λ_{eff} = 0.54 μ) overlaps both the red (λ_{eff} = 0.59 μ) and violet (λ_{eff} = 0.45 μ) filter band passes, we divided the red mosaic by the violet mosaic pixel by pixel to obtain maximum color information. The

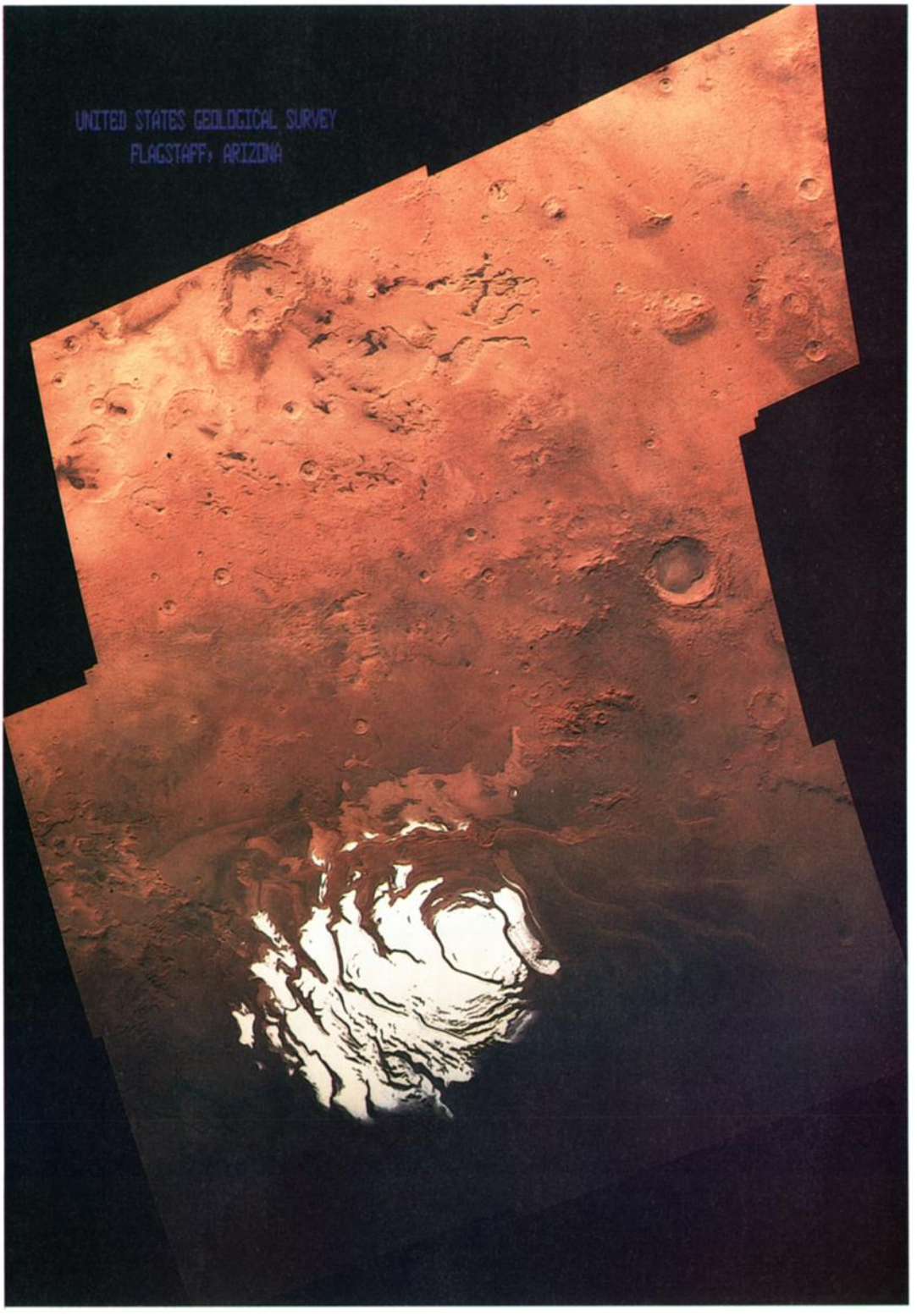

Plate 1. Viking Orbiter 2 rev 407 (L_s = 341°) color mosaic of the south polar region, with 500 m/pixel resolution. Orthographic projection with 0°W longitude is at 12 o'clock; the Sun is toward 11 o'clock.

resulting red/violet (*R/V*) mosaic is shown in Figure 1. Errors in registration of the color mosaics (relative to each other) are not greater than 5 pixels, as indicated by the bright rims around the polar cap. Despite the presence of atmospheric scattering distinct surface units can be recognized in the *R/V* mosaic. All of the surface units examined in this study are red in color, but we shall refer to the units that are less red as "neutral" in color. Near the top of the mosaic, neutral and darker material appears in topographic depressions that can act as natural saltation traps. The polar cap

Fig. 1. Rev 407 red/violet ratio image. Black corresponds to a ratio of 1.7, white is $R/V = 2.8$. The bright lines bordering the polar cap are due to slight misregistration of the two mosaics. Seams between individual images in mosaic are visible because of offsets of up to 10%.

and outliers of seasonal frost appear black ($R/V \leq 1.7$) in this rendition of the mosaic, but they are actually slightly red in color, in part because of atmospheric scattering. Variations in the color of the surface of the layered deposits are also evident and will be described in detail in the next section.

By measuring the brightness observed in shadows, we can estimate the component of brightness due to atmospheric dust scattering at various points in the mosaic. Over 100 of the shadow brightnesses we measured are shown in Figures A1–A3, along with model fits described in the Appendix. The uncertainty in the absolute calibration of the television data, mainly due to the uncertainty in dark current subtraction, can be significant in evaluating atmospheric brightness. The error in dark current subtraction is greater at low raw data values, so that shadow brightnesses near the bottom of the mosaic are the most uncertain. Error bars of 13% are plotted in Figures A1–A3, illustrating the absolute uncertainty in the shadow data except near the terminator, where the error is larger. While determination of the dust-scattering parameters (as described in the Appendix) is sensitive to errors in

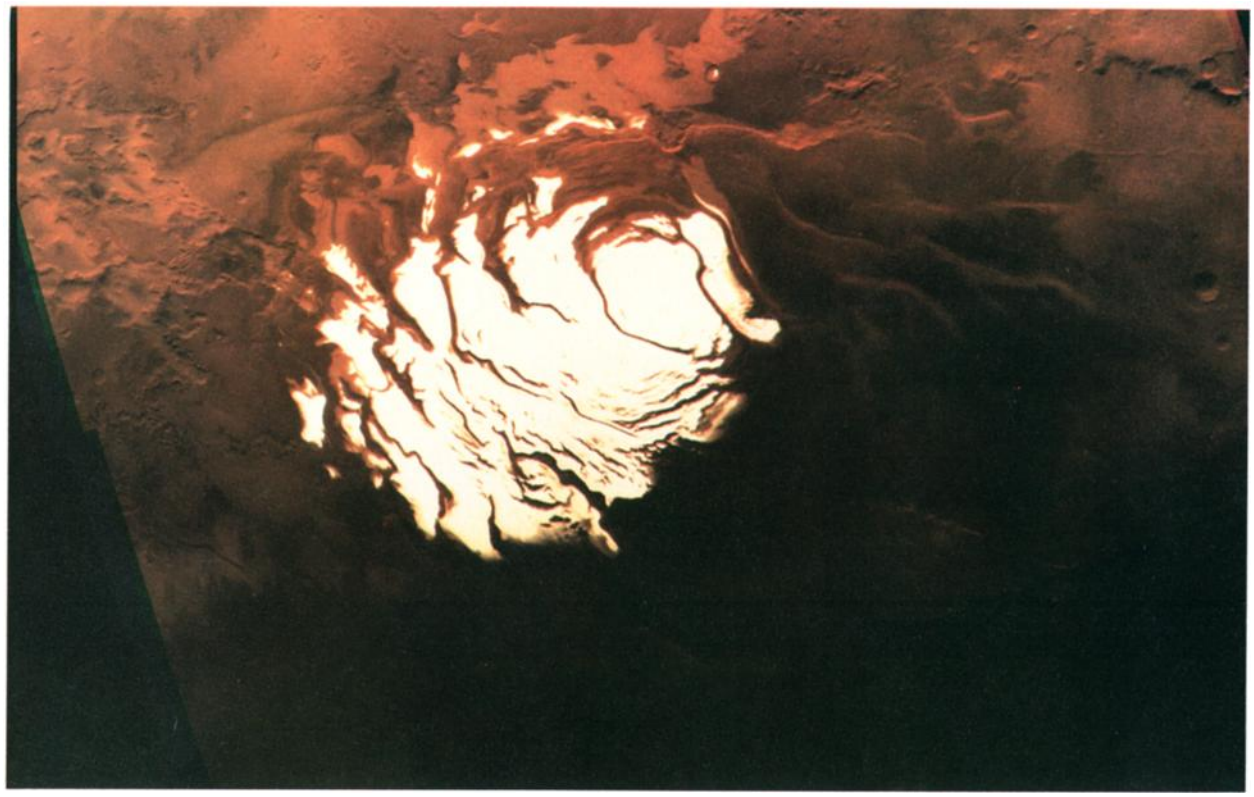

Plate 2. Part of rev 407 color mosaic, corrected for atmospheric scattering. Note albedo variations in layered deposits near the polar cap. The area shown is 1200 km across. The vicinity of the polar cap near bottom is shown in detail in Figure 4.

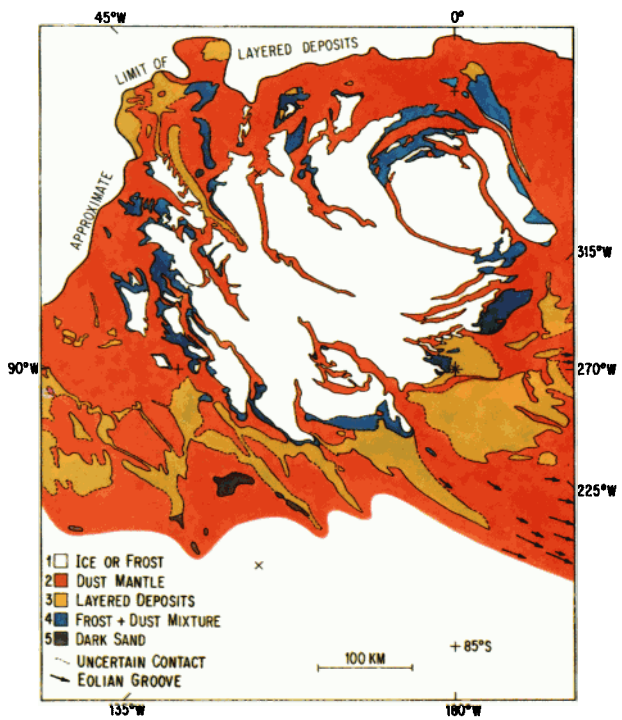

Plate 3. Map of color/albedo units in the south polar layered terrain, originally mapped at 1 : 2,000,000 scale. Drafted lines are located to accuracies of a few kilometers or better. Dashed lines represent uncertain or gradational contacts.

absolute calibration, delineation of surface color/albedo units is limited only by noise in the data. The signal/noise ratio is too low to identify surface units only in the bottom right corner of the mosaic.

The lower portion of the mosaic, where the layered deposits appear, was corrected for atmospheric scattering (Plate 2) and used to create the R/V mosaic shown in Figure 2. The atmospheric brightness and attenuation at selected points in the mosaic were predicted using 2.5-μ radius particles [*Pollack et al.*, 1979] with the scattering properties given in Table 2. The best fit model (normal optical depth = 0.13) was run at 35 points in a 400 × 400 pixel grid; then bilinear interpolation was used to approximate the atmospheric brightness and attenuation at every other pixel in each color mosaic. The interpolated atmospheric brightness was subtracted from each pixel value, and the result was divided by the total attenuation of the incoming and outgoing radiation to approximate the atmosphereless reflectance of the surface.

The R/V and color mosaics were used to identify five color/albedo units in the layered terrain. The units were mapped (Plate 3) where the noise level in the mosaics is sufficiently low using an overlay on the 1 : 2,000,000 photomosaic shown in Figure 3. *Tanaka and Scott* [1987] mapped the area at the top of Plates 2 and 3 and Figure 2 as layered deposits, but we find no evidence of layering in that area, either in the digital mosaics used here, in the 1 : 2,000,000 photomosaic, or in high-resolution Mariner 9 images of the area. This area may be an exposure of the basal member(s)

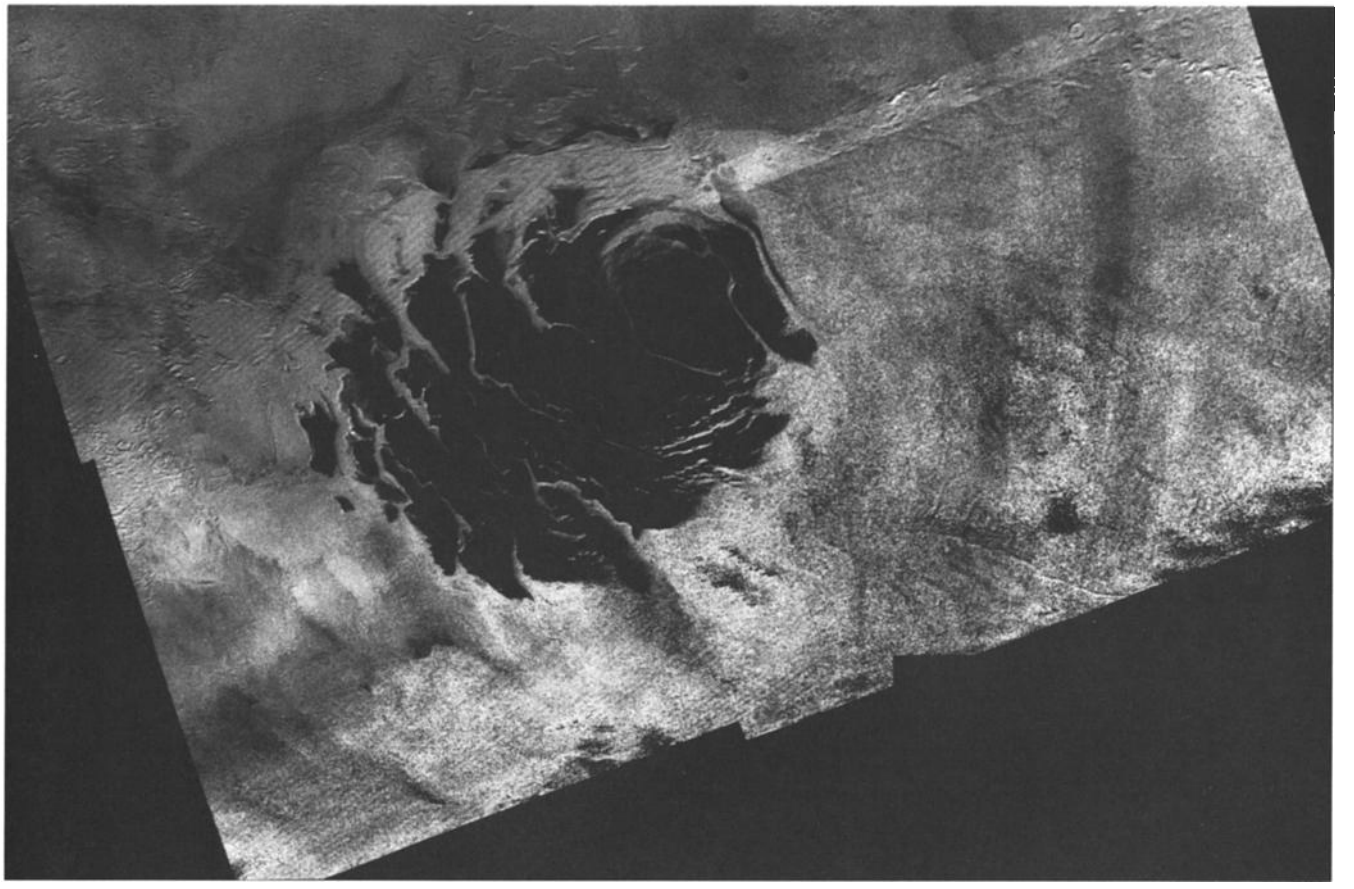

Fig. 2. Red/violet ratio mosaic, corrected for atmospheric scattering. The signal/noise ratio is rather low at the bottom and at the right side of the mosaic.

of the layered deposits or a separate unlayered unit. For the purposes of this paper we define "layered deposits" as those units in which distinct layering can be seen. Our primary interest is in the layered deposits, so we have chosen to map only the area within the layered deposits and polar cap, as delineated in Plate 3. Some areas in the layered deposits have the same color and albedo as areas outside the layered terrain, but we have subdivided only the layered deposits.

Contacts between color/albedo units were located on both the *R/V* mosaic and the photomosaic and have been drafted to an accuracy of a few kilometers or better (mosaic resolution is 0.5 km/pixel). The five surface color/albedo units (and corresponding interpretations) are (1) bright neutral (polar frost), (2) bright red (dust), (3) dark red (layered deposits), (4) bright intermediate (mixture of units 1 and 2), and (5) dark neutral (sand). The *R/V* ratios of unit 4 are similar to those of unit 3, but the two units may be distinguished by their overall albedos: unit 4 is brighter than the other units (except unit 1), while unit 3 is slightly darker than unit 2 (Table 1). Because of the variation in illumination across the mosaic, the average reflectances of selected 5 × 5 pixel areas were divided by the cosine of the incidence angle to facilitate comparison. The resulting Lambert albedos (Table 1) are not comparable to the albedos used in the atmospheric scattering model (Appendix) because the assumption of a Lambert photometric function is incorrect in general. The unit map shows that many of the contacts between these units are gradational, as would be expected where sand or dust cover is incomplete or where relative amounts of dust and frost vary. The location of contacts is uncertain where the signal to noise ratio is low (at the bottom of the mosaic). However, some of the contacts between the frost or frost mixtures (unit 1 or 4) and the surrounding darker units are quite sharp, probably because of topographic control of their boundaries.

Surface albedos higher than the values of 0.09 (violet) and 0.25 (red) used in the atmospheric model must be used to correct for atmospheric effects over areas of bright frost. Frost albedos of 0.5 (violet) and 0.6 (red) were used to model the atmospheric reflectance over several points in the polar cap. Similarly, surface albedos of 0.15 (violet) and 0.35 (red) were used to correct for atmospheric scattering over unit 4. The above surface albedos were estimated from the brightness contrast between the bright units and the surrounding areas and adjusted iteratively to approach the color of the corrected data. The *R/V* ratios of these higher surface albedos (frost = 1.2; unit 4 = 2.33) are consistent with the *R/V* ratios of the corrected surface data, as indicated in Table 1. The lower surface albedos yield slightly higher corrected *R/V* ratios because the redness of the surface reflection is overestimated.

3. Results and Interpretations

We have applied a multistream radiative transfer model to a Viking Orbiter color mosaic of the south polar region. The parameters used in the model are similar to those found by

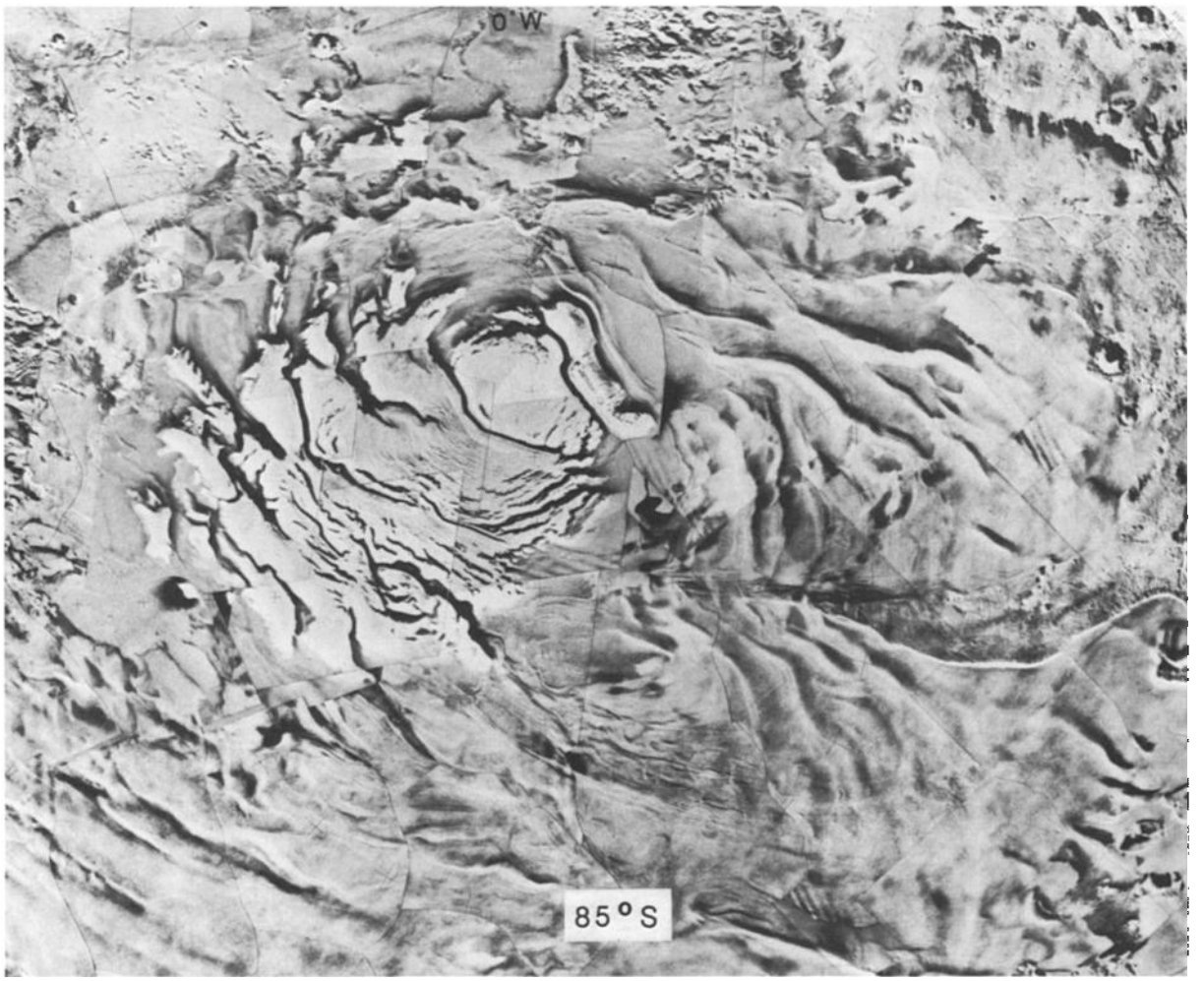

Fig. 3. Section of U.S. Geological Survey controlled photomosaic MC-30 A/B (I-1647), original scale = 1 : 2,000,000. Note the off-cap eolian grooves at bottom, deflected left by Coriolis force. The south pole is just below and left of center.

other workers: normal optical depth = 0.13; single-scattering albedo = 0.57–0.85; asymmetry parameter = 0.31–0.49; extinction efficiency = 2.64–2.75 with 2.5-μ particles; and surface albedos of 0.09 (violet), 0.18 (green), and 0.25 (red). This model should also be valuable for future photometric measurements of the Martian surface and atmosphere.

In the absence of any wavelength dependence in the photometric function and neglecting the difference in color between the surface and the atmospheric scattering, topography should vanish in an *R/V* ratio image. However, some topographic features are still visible in the *R/V* image (Figure 1), and there is an overall decrease in the *R/V* ratio (from 2.6 to 1.8) with increasing incidence angle. *Guinness* [1981] found that the color of the soil at the Viking Lander 1 site depends on phase angle, but since phase variations in the mosaic used here are less than 5°, the overall *R/V* gradient cannot be explained by phase-dependent color variations. Dust scattering in the atmosphere contributes to the overall *R/V* gradient (from top to bottom) in Figure 1, as indicated by the shadow data described in the Appendix. As we demonstrate below, the appearance of topographic features in Figure 1 is also due to atmospheric scattering.

The mountains at right center and Sun-facing scarps in Figure 1 are more red on their northern (sunward) slopes. This phenomenon is due to the contribution to illumination of the surface by diffuse, relatively "bluer" atmospheric

TABLE 1. Lambert Albedos and Colors of Surface Units

Unit	Interpretation	Violet	Red	*R/V*
1	frost	0.18–0.43	0.27–0.53	1.2–1.6
2	dust mantle	0.04–0.05	0.14–0.18	3.2–3.8
3	layered deposits	0.03–0.05	0.10–0.13	2.5–3.2
4	mixture of units 1 and 2	0.05–0.09	0.14–0.21	2.2–2.9
5	dark material	0.02–0.05	0.04–0.10	1.8–2.1

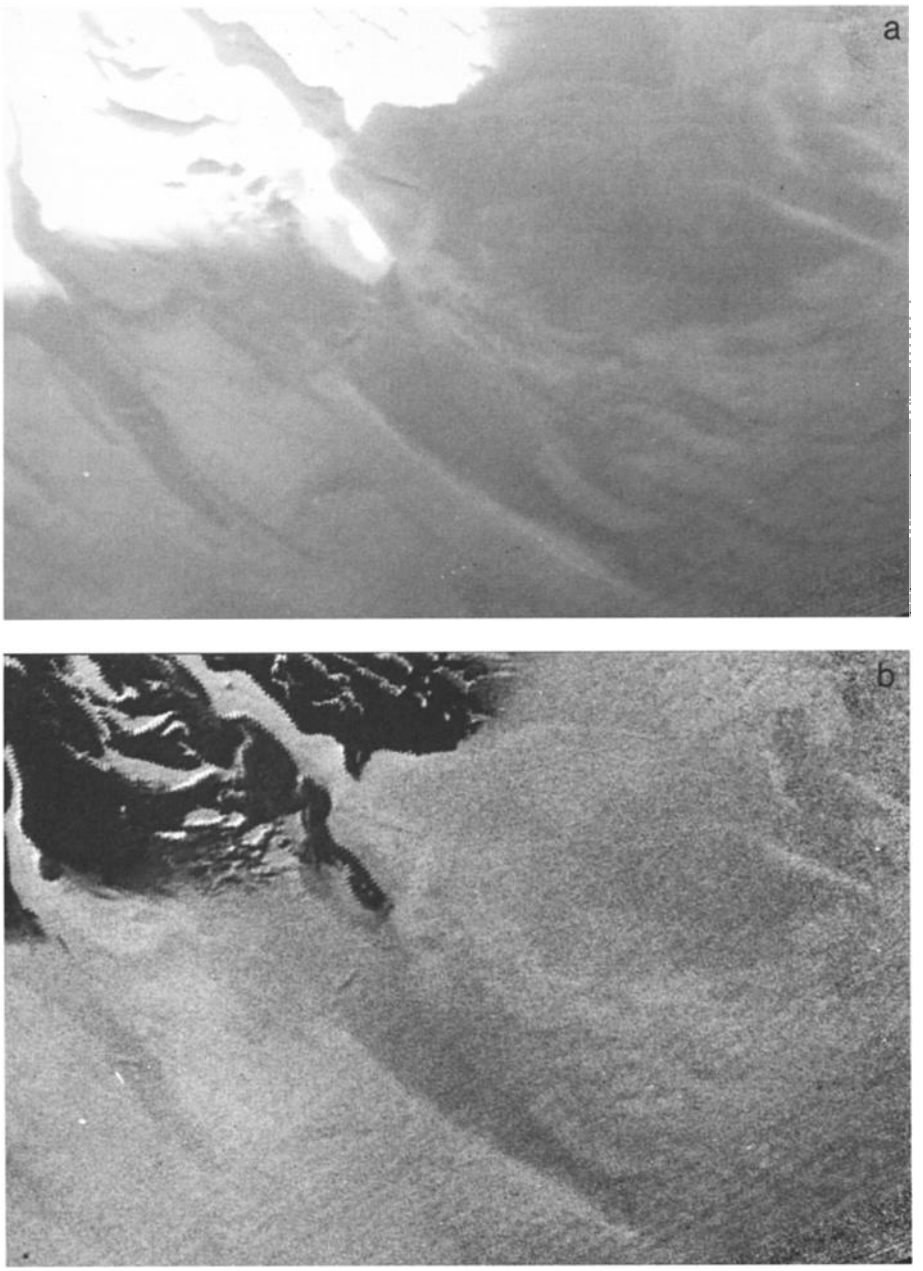

Fig. 4. Detail of the vicinity of the south pole, with frost cap at top: (*a*) portion of red mosaic showing elongate areas of lower albedo (unit 3) and (*b*) portion of red/violet ratio mosaic showing that darker areas (unit 3) are also less red.

scattering. As shown in the Appendix, the R/V ratio of atmospheric scattering in shadows is about 2.0, while the surface R/V ratio is close to 3.0. Increased direct solar reflection on sunward facing slopes increases the R/V ratio of the total reflected radiation relative to adjacent level areas, where reflected diffuse atmospheric illumination is a larger fraction of the total. The variation in R/V with incidence angle is no longer evident when the effects of atmospheric scattering are removed. An area near the top of the mosaic (at about 68° incidence angle) was corrected for atmospheric effects using the model described in the Appendix. Dark material in topographic depressions in this area has R/V = 1.7–2.1, similar to dark material (unit 5) at higher incidence angles. The plains in the low-incidence region have R/V ratios between 3.0 and 3.5, similar to the plains at the top of Figure 2 at about 77° incidence angle. Occasional bright areas at low incidence have R/V = 3.6, comparable to the dust in the layered terrain (unit 2).

Examination of the R/V mosaics (see Figure 2) shows no detectable color change between the layered deposits and the surrounding unfrosted terrain. In particular, the boundary of the layered deposits cannot be seen at the left and right sides of Figure 2. This lack of contrast indicates that the surfaces of the layered deposits and the surrounding terrains are composed of the same material or that there is a dust mantle covering the entire area. As we will discuss below, there is morphological evidence suggesting that a dust mantle has been stripped away in some places.

The R/V ratio of unit 2 varies from 3.3 to 3.8 where the noise level in the mosaic is low. Darker, more neutral ($R/V \approx$

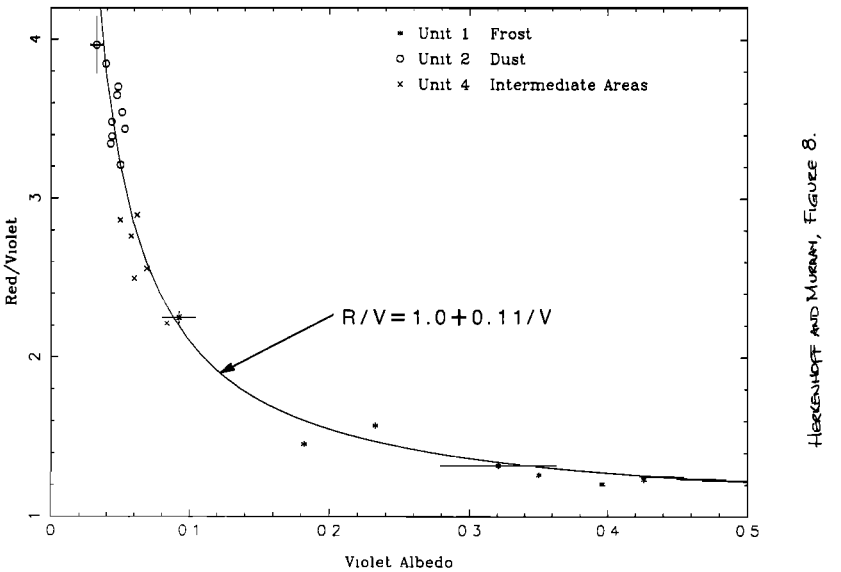

Fig. 5. Red/violet ratio versus violet Lambert albedo for representative points in 3 surface units in the vicinity of the south polar residual cap. The model curve is discussed in the text. Error bars represent 13% uncertainty in absolute albedos, the typical sampling noise in 5 × 5 pixel areas in *R/V* mosaic.

2.9) areas of unit 3 occur throughout the layered deposits and in many cases appear to be associated with eolian erosional features. Unit 3 cannot simply be an exhumed flat-lying dark layer, because significant relief can be seen within a large area of the unit near 89.5°S, 200°W (Figures 3 and 4). Although this unit may represent a mantling of darker, more neutral material, we consider it more likely that this area has been stripped of its dust mantle by winds blowing off the polar cap. In Figure 3, linear grooves can be seen cutting across complexly terraced landforms, suggesting extensive wind erosion [*Cutts*, 1973]. These grooves are parallel to the elongate areas of unit 3 below the polar cap (in Plate 3) but are mostly coated by the dust mantle (unit 2). Evidently, the cutting of the grooves was followed by deposition of the dust mantle, which has been partially removed elsewhere by further eolian activity. A layer of dust only about 10 μ thick should be sufficient to conceal the underlying bedrock. We conclude that unit 3 represents exposures of layered deposit "bedrock" that are darker and less red than the dust mantle that covers much of the area. The *R/V* of unit 3 is the same as that of the north polar layered deposits, as reported by *Thomas and Weitz* [1989].

The occurrence of bright, less red areas (unit 4) adjacent to the polar frost cap (unit 1) suggests that these areas are mixtures of frost and red dust (unit 2) below the resolution of the images. Mariner 9 returned the first high-resolution pictures of the south poiar region, showing incomplete frost cover within the residual cap at a variety of spatial scales [*Murray et al.*, 1972]. Although variegation in the frost cap is also evident in the mosaics used here, the details of the frost distribution are not indicated in Plate 3 for simplicity. Violet Lambert albedo is plotted against the *R/V* ratio in Figure 5, where atmospheric scattering has been removed. The data are fit well by a model that assumes linear mixing of two color components below the image resolution: $R/V = A_1 + A_2/V$, where A_1 and A_2 are constants dependent upon the color and albedo of pure frost (unit 1) and pure dust (unit 2), and R and V are the red and violet Lambert albedos, respectively. This model calculates the consequence of a macroscopic dust/frost "checkerboard" with possible length scales from millimeters to 100 m (the resolution of the best images). A least squares fit of the data in Figure 5 gives $A_1 = 1.0$ and $A_2 = 0.11$, comparable to the values given by *James et al.* [1979] for mixtures of seasonal frost and bare ground: $A_1 = 1.257$ and $A_2 = 0.105$. The residual cap has an *R/V* ratio of about 1.2, similar to the *R/V* of 1.25 found by *James et al.* [1979]. Evidently, the frost in unit 4 is less red than the seasonal frost observed during the spring, resulting in a decrease in A_1 with time. This is consistent with the temporal brightening of the south polar seasonal cap [*Kieffer*, 1979; *Paige*, 1985] due to dust removal or sinking of dust grains into the frost.

Unit 4 appears to be the surface expression of a deposit that is younger than the surrounding layered terrain: secondary craters from a 17-km impact crater at 84.5°S, 359°W [*Plaut et al.*, 1988] are present in the layered terrain, but they "are either much rarer or more muted" [*Howard et al.*, 1982, p. 200] in the area of unit 4 at 84.8°S, 356°W. This unit has apparently been deposited since the impact that produced the secondary craters [*Howard et al.*, 1982]. Perhaps the persistence of seasonal frost in this area late into the summer (due to a regional poleward slope or to small topographic depressions) allows entrained dust to remain throughout the year, rather than being removed by winds. The net annual accumulation of small amounts of dust trapped in this manner might produce the observed young deposit if continued for many seasonal cycles. The thickness of dust and/or frost needed to produce the observed burial of the ≤2-km-diameter secondary craters is at most a few hundred meters, assuming depth/diameter is approximately equal to 0.2 [*Pike*, 1979].

A large area of similar brightness and *R/V* ratio (not mapped in Plate 3) appears around 83°S between roughly 0° and 30°W. This bright area is commonly occupied by an outlier of seasonal frost early in the southern summer and was interpreted by *James et al.* [1979, p. 2905, Figure 27] to

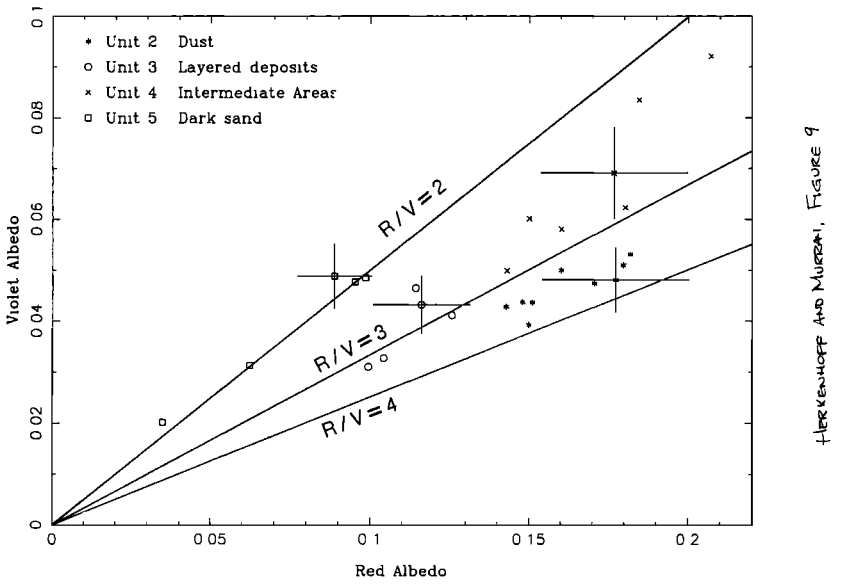

Fig. 6. Violet versus red Lambert albedo for 4 surface units in the vicinity of the south polar residual cap. Error bars represent 13% uncertainty in absolute albedos.

be "due to dust entrained during the condensation process." While we agree that dust deposits are probably stabilized by surface volatiles, our analysis of the color and albedo of this unit indicates that the presence of frost below the limit of resolution is responsible for its high albedo. This area may also be a site of recent deposition.

Unit 5 is the darkest and most neutral in color of the units found in the south layered deposits. It is found only in what appear to be topographic lows, suggesting that it may be composed of sand-sized particles caught in saltation traps. Material of the same color ($R/V \approx 1.9$) is found in craters and other depressions in the upper part of Plate 1, indicating that it is widespread and has therefore probably been transported by winds. *Thomas and Weitz* [1989] found a similar R/V ratio for the north polar erg. The presence of dark material (unit 5) at the downwind ends of some exposures of unit 3 (Figure 5) suggests that saltation aids in the removal of the dust mantle.

The source of the dark material (unit 5) is not evident in the data used here. If the source of the dark material is not the layered deposits, it must have been transported into the layered terrain from more equatorial areas by saltation or suspension. The current Martian atmosphere cannot support grains larger than about 50 μ in suspension [*Arvidson*, 1972], and extensive transport and deposition of dust from suspension are unlikely for particles larger than about 10 μ. Alternatively, the dark material may be composed of fluffy particles [*Saunders et al.*, 1985, 1986], but such particles still must have saltated to become trapped in topographic depressions if they were deposited initially from suspension. Saltating grains would be expected to erode any dust mantle, so that transport of the dark material into the layered terrains could not have occurred since the deposition of the dust mantle. If the dark material was deposited before the dust mantle, it would not be apparent today unless the dust was able to trickle down into the open spaces between particles or was injected into suspension by local saltation of the larger particles. Particles 100 μ in size are the most easily saltated under current Martian atmospheric conditions, while 10-μ particles require about twice the wind velocity to initiate saltation [*Greeley et al.*, 1980]. The dust particles are probably less than 10 μ in diameter, so that if the dark material consists of ~100-μ particles, they may have been cleaned of dust by local saltation. Therefore unit 5 could have been transported from a source outside the layered terrain and deposited before the dust mantle.

Conversely, the source of unit 5 may be local but not obvious in the images used here. The genetic relationships between scarps and dune fields can be inferred from high-resolution Viking north polar images [*Thomas and Weitz*, 1989] but are not resolved in the lower-resolution south polar data used here. The hypothesis that the dark material is eroded from the layered deposits [*Thomas and Weitz*, 1989] is supported by the color and albedo of units 2, 3, and 5 (Figure 6). The color/albedo of the layered deposits (unit 3) is intermediate between that of dust (unit 2) and that of dark material (unit 5), consistent with their being a mixture of dust and dark material. The dark material therefore may have originated locally within the layered deposits.

4. Discussion

Before we discuss the implications of our results in conjunction with previous work, we must state our inherent assumptions. The lateral extent and constant thickness of individual layers suggest that the layered deposits were formed by eolian deposition; we consider only such processes. Despite the significant differences in the size, appearance, and setting of the north and south layered deposits, we assume that their origin and evolution were similar. The current contrast may be due to the north/south asymmetries in Martian topography and climate (Mars' orbital eccentricity is rather high now). The variable climate presumably controls the relative and overall effects of the depositional and erosional processes common to both hemispheres. We accept the "conventional wisdom" that water ice plays an important role in the formation of the layered deposits and assume that solid H_2O cements the darker (presumably silicate) particles together. Finally, we exclude the possibil-

ity that periodic volcanic eruptions have caused most of the layering, although this mechanism cannot be ruled out completely.

If the south polar layered deposits are composed only of bright red dust and ice, their color and albedo suggest that ice is not abundant at the surface, since the layered deposits are darker than the dust that mantles them. However, *Clark and Lucey* [1984] have shown that there is very little change in visual reflectance of soil and ice mixtures with increasing soil content for soil fractions above ~1% by weight. It is not clear from their data what effect (if any) adding small amounts of ice to the soil has on the visual reflectance of the mixture. A little ice could even make the soil appear darker, as it did in their experiments with bright kaolinite. Clearly, the albedo of the layered deposits is not a reliable measure of their ice content.

In any case, calculations of the stability of water ice in the polar regions of Mars [*Toon et al.*, 1980; *Hofstadter and Murray*, 1989] indicate that water ice should not currently be present at the surface of the layered deposits. This implies that the observed color/albedo ratio of the layered deposits must be due to nonvolatile components.

We now consider four hypotheses for the composition of the layered deposits, all presuming that water ice is the cementing material but does not affect the observed reflectance. The widely held notion that the layered deposits are composed of only dust and ice is discussed, along with some alternatives for the source of the dark saltating material. We then discuss the possibility of only dark sand and ice in the layered deposits and finally consider a mixture of dust and dark sand.

4.1. *Dust Only*

The first possibility that we consider is that the dark, saltating material (unit 5) is a sublimation product of the layered deposits, which are composed only of bright dust and ice. This hypothesis was proposed by *Saunders et al.* [1985], who invoked dark carbonaceous meteoritic dust (which is probably unstable under oxidizing Martian surface conditions) to coat and darken the saltating filamentary sublimation residue (FSR) particles derived from erosion of the layered deposits. Their mechanism cannot explain the presence of dark material near its source, however, as saltation across an area with dark dust at the surface is required. The FSR particles have roughly the same albedo as the dust from which they are made, although neither the reflectance properties of the FSR nor the dust that was used to make them were measured quantitatively (A. Storrs, personal communication, 1989). *Thomas and Weitz* [1989] showed that dark material is present very near to its apparent source in the north polar layered deposits, implying that the dark material is already dark upon erosion. Although the FSR may be somewhat darker than the dust from which it forms, it is unlikely that this process can produce particles that are at least 3 times darker in red light than the dust mantle (Table 1).

Formation of the dark dunes from erosion of layered deposits composed only of dust and ice by this mechanism is therefore implausible unless there is a second, darker type of dust in the layered deposits as well. A (possibly minor) dark component of dust could preferentially form FSR and therefore dark saltating material, leaving the bright dust to be injected into suspension and removed. *Pollack et al.* [1977, 1979] found that the Viking lander sky brightness measurements are consistent with the existence of ~1% magnetite ($Fe^{2+}Fe_2^{3+}O_4$) in the atmospheric dust. *Hargraves et al.* [1979, p. 8383] noted that the reference test chart magnet on Viking Lander 1 continued to attract magnetic particles from the atmosphere during the extended mission and suggest that maghemite (γ-$Fe_2^{3+}O_3$) is the most likely candidate for the magnetic material. They conclude that "the results of *Pollack et al.* [1977] may not be inconsistent with the presence of a slightly ferroan maghemite" in the Martian atmosphere. About 1–7% of the soil at the Viking lander sites is magnetic [*Hargraves et al.*, 1979], suggesting that more dark magnetic material may be carried in suspension during epochs of greater atmospheric pressure. If magnetite motes are transported by suspension into the polar regions, incorporated into the layered deposits and eventually eroded, magnetite may form FSR particles either alone or mixed with phyllosilicate dust, perhaps aided by its magnetic properties (A. Storrs, personal communication, 1989). Such dark particles may then saltate to form the dunes that probably represent 1–10% of the eroded volume of the layered deposits [*Thomas*, 1982]. An attempt to form FSR from magnetite or maghemite dust has not been made (E. Laue, personal communication, 1989), but if FSR can be formed using these minerals, it would probably be dark. Hence erosion of magnetite or maghemite particles in the layered deposits could conceivably account for the dark dunes described by *Thomas and Weitz* [1989], and the albedo of unit 3 (intermediate between dust and dark material (Figure 6)) may be due to a concentration of dark material at the weathered surface of the deposits.

Storrs et al. [1988, p. 510] argue that "the low thermal conductivity of the FSR . . . seems inconsistent with the thermal inertia" of the polar dunes, which is no greater than 6.5×10^{-3} cal cm^{-1} $s^{-1/2}$ K^{-1} [*Paige and Kieffer*, 1987]. Using the density and thermal conductivity of montmorillonite FSR given by *Storrs et al.* [1988] and the mean specific heat of various silicates (0.14 cal g^{-1} K^{-1} at 220 K) given by *Winter and Saari* [1969], a thermal inertia of 2×10^{-3} is indicated for the FSR. The presence of the Martian atmosphere and even small amounts of water ice will tend to increase the thermal conductivity of the FSR. Given that *Paige and Kieffer* [1987] regard their thermal inertia of the polar dunes as an upper limit and that the thermal conductivity of the FSR in a good vacuum (A. Storrs, personal communication, 1989) is greater than the thermal conductivities at low ambient pressure of a wide range of rock powders and sands measured by *Wechsler and Glaser* [1965], we do not feel that the thermal conductivity of the FSR and the thermal inertia of the polar dunes are inconsistent. We conclude that the possibility of the polar dunes' being composed of FSR particles cannot be excluded on the basis of thermal inertia data.

4.2. *Sand From External Sources*

The source of the dark material may not be the layered deposits, however. It is possible that dark sand partially or completely covers the layered deposits periodically and is removed when the polar wind patterns change. The main problem with this hypothesis is that dark dunes appear to have sources in the north polar layered deposits [*Thomas*,

1982; *Thomas and Weitz*, 1989]. In addition, this concept does not reconcile the difference between the albedos of the dust mantle (unit 2) and the layered deposits (unit 3). The Mars Observer camera may be able to obtain images that will allow detailed study of the scarps in the layered deposits and their relationships to the adjacent dune fields. Since the available images indicate that dark material is being eroded from the north polar deposits and forming dunes [*Thomas*, 1982], we prefer hypotheses that are consistent with the layered deposits being the source of the dark saltating material.

4.3. *Sand Only*

Could the layered deposits be composed of dark sand and ice only? As stated above, large amounts of ice are not expected to be present at the surface of the layered deposits, so that their albedo must be due to nonvolatile material. Because the layered deposits appear brighter than the dark saltating material in both polar regions, we feel that it is unlikely that the layered deposits are composed only of dark material and ice.

4.4. *Dust and Sand Mixture*

Perhaps the layered deposits are made up of a mixture of dust, dark sand, and ice. The question then is how could sand become incorporated into the layered deposits? *Thomas and Weitz* [1989] conclude that only small amounts of sand in the north polar deposits are required to produce the observed dunes. We agree with their assertion that it is unlikely that sand could be carried in suspension, even by a much denser Martian atmosphere, and that sand must therefore be transported to the polar regions by saltation. The problem is how to deposit dust and sand simultaneously, as saltating sand will inject dust into suspension, carrying it away from the surface. Perhaps the dust is codeposited with water ice and effectively cemented to the surface by solid H_2O. Then sand could saltate over the polar cap, becoming trapped in topographic depressions. The entire layered deposits may have been covered periodically by a thin sand sheet, but laterally continuous saltating sheets of such constant thickness are not found on Earth and are probably also unlikely on Mars. It is more likely that if sand is present within the layered deposits, it is in patches a few meters in size at most and is therefore undetectable in even the best Viking images. Such a mixture can account for the color and albedo of the layered deposits (unit 3) with respect to the dust mantle (unit 2) and the dark material (unit 5).

4.5. *Genetic and Climatic Implications*

We now consider the implications of the compositional hypotheses discussed above for the formation of the layered deposits, along with the variations in climate or circulation that are required for them to function. Two hypotheses that include dark material in the layered deposits are preferred and reconcile the available observations: (1) bright dust, dark dust, and ice; and (2) bright dust, dark sand, and ice.

The dust and ice scenario involves formation of sublimation residue particles that saltate to form the dark dunes adjacent to the layered deposits. Since dark dust seems required to form dark FSR particles, we propose that magnetite or maghemite dust is deposited from suspension onto the layered deposits. The dust in the atmosphere over the Viking landers contains about 1% opaque phase [*Pollack et al.*, 1979], while the soil contains 1–7% magnetic material [*Hargraves et al.*, 1979]. For comparison the volume of dark dune deposits in the polar regions is estimated to be 1–10% of the eroded volume of the layered deposits [*Thomas*, 1982]. This comparison suggests that dark magnetic material is incorporated into the layered deposits in the same proportion as in surface fines and therefore that the dark material is easily transported by winds. Since the percentages of dark material given above are essentially identical (considering the uncertainties involved), it is conceivable that layered deposits may be forming in the current climatic conditions.

If sand is mixed into the layered deposits, a poleward flow is necessary to transport the sand onto the polar deposits. *Thomas* [1982] found that winds tend to blow off of the north polar cap, but the circulation pattern is rather complex. Sand is not expected to saltate during the winter and early spring when the dunes are covered by seasonal CO_2 frost, so that the summer circulation is most important to the net transport of sand. It appears, then, that sand is not currently being transported onto the north polar cap and that a change in circulation is needed to bring sand into the layered deposits [*Thomas*, 1982]. Periods of high obliquity may result in the disappearance of the residual caps and enable saltation of sand across the layered deposits during the summer.

5. SUMMARY AND CONCLUSIONS

Five albedo/color units have been identified and mapped in the south polar layered deposits, including polar frost. Much of the south polar region appears to be mantled by material (probably dust) with R/V ratios between 3.2 and 3.8. Eolian erosion of linear grooves near the south pole was followed by deposition of the dust mantle. This mantle has been removed (presumably by off-cap winds) from certain areas in the layered deposits, exposing slightly darker, less red "bedrock." Measured layered deposit colors and albedos lie between those of the dark material and those of the dust mantle, consistent with the layered deposits being a mixture of dark material and bright dust.

A bright, neutral unit, adjacent to the polar cap, is a mixture of frost and bare ground below the resolution of the images. Frost/ground patchiness on a horizontal scale of less than about 100 m is indicated in these areas. *Thomas and Weitz* [1989] found a similar unit in the north polar deposits. In at least one area this unit appears to be younger than the surrounding layered terrain, perhaps because of the trapping of dust by seasonal frost. A large area of similar color and albedo just outside of the layered terrain, the site of an outlier of seasonal frost, may also be undergoing deposition. The Mars Observer camera should be used to attempt to resolve patches of frost and bare ground in these areas.

Darker, more neutral saltating material is occasionally present in topographic depressions in the layered deposits and elsewhere in the south polar region. The source of this dark material is not evident in the data considered in this paper, but it may be local. If the source is not local, the lack of dust mantling these dark deposits is paradoxical. A possible resolution of this paradox may be that the dark deposits are composed of larger (~100 μ) particles that are more easily moved by winds than the micron-sized dust that forms the mantle [*Iversen and White*, 1982]. In this case,

local saltation of the dark material since the deposition of the dust mantle could allow the dust to settle between dark grains and out of view or could eject dust into suspension. Again, the Mars Observer camera should be used to obtain high-resolution images of areas of dark material in the southern layered deposits and study them in detail. Such data may indicate the source of the dark material.

While much of the south polar layered deposits appear to have been at least partially eroded, deposition has occurred recently in some areas near the residual cap. The geologic history of the south polar layered deposits is therefore rather complex, with deposition occurring in areas where frost lingers late into the summer and eolian erosion of the dust mantle occurring in other areas.

Under the assumptions that the layered deposits are eolian in origin and that the evolution of the north and south deposits are similar, we conclude that the layered deposits are probably composed of dust and ice, with small amounts of dark dust or sand. In the case of dark sand, climatic changes seem necessary to provide a net poleward wind regime, enabling sand to saltate into the layered deposits. Only medium-resolution color data are used here, and analysis of high-resolution Mariner 9 images of the south polar region is in progress.

We look forward to the acquisition of Mars Observer data that will test the hypotheses described here. Mars Observer's polar orbit enables repeated coverage of the polar regions and is ideally suited to detailed study of the polar layered terrains. Although data returned by the deselected visual and infrared mapping spectrometer would probably have constrained the composition of the polar deposits better than any of the remaining instruments, the mission as currently planned should be able to address important questions regarding the layered terrain. As mentioned above, the high-resolution camera will be able to examine in detail the geological relationships among the units described in this paper. The radar altimeter will yield essential topographic information, and the gamma ray spectrometer may estimate the amount of H_2O near the surface. Finally, the thermal emission spectrometer and/or the pressure-modulated infrared radiometer may be able to distinguish sand from FSR particles in the dark material. Such observations will provide crucial tests of the hypotheses proposed here.

APPENDIX: ATMOSPHERIC SCATTERING MODEL

Analysis of the surface properties of Mars is complicated by the presence of dust in the Martian atmosphere. The determination of surface albedos and application of photoclinometric techniques, for instance, require accurate removal of the atmospheric component of brightness. We have modeled dust scattering in the south polar region with a radiative transfer program described in detail by Michelangeli, D. V., M. A. Allen, Y. L. Yung, R.-L. Shia, and D. Crisp (Enhancement of atmospheric radiation by an aerosol layer, submitted to *Journal of Geophysical Research*, 1990). The program uses the multistream Feautrier formulation for an inhomogeneous plane-parallel atmosphere with a single Henyey-Greenstein phase function. It assumes Lambertian scattering at the surface, and we have modified the code to account for the sphericity of the planet when calculating the incoming solar radiation. The plane-parallel assumption is unacceptable at high emission angles, but only moderate emission angles are modeled here. The program calculates the total radiation observed for a given viewing geometry, as well as the attenuation of the downgoing solar and upgoing reflected radiation. The atmospheric component, including diffuse flux reflected from the surface, is calculated by subtracting the Lambert surface reflection from the total. Rayleigh scattering in the Martian atmosphere is insignificant compared to dust scattering [*Kahn et al.*, 1981] and was therefore not considered in this model.

In order to limit the number of variable parameters in the model we have made use of published results regarding Martian dust scattering. Our model has nine altitude levels up to 50 km, the maximum dust height having been approximately determined using Viking Orbiter limb images [*Jaquin et al.*, 1986]. The dust concentration decays exponentially with a scale height of 10 km, as inferred from Viking Lander observations by *Pollack et al.* [1977]. The extinction efficiencies Q_{ext} given in Table 2 were taken from *Pollack* [1982]. Since the 2.5-μ (cross-section weighted mean radius) dust particles are forward scattering [*Pollack et al.*, 1977], 12 azimuthal harmonics were used in the calculation. The error in approximation of the phase function is less than 7% for an asymmetry parameter of 0.55 and decreases as scattering becomes more isotropic. Use of a greater number of azimuthal harmonics does not significantly affect the results.

The remaining parameters to be determined are the optical depth τ, the single-scattering albedo ω_0, the Henyey-Greenstein asymmetry parameter g, and the surface reflectance r_0. Viking Lander observations show that τ is rarely less than 0.2 [*Pollack et al.*, 1977], while Viking Orbiter images have been used by *Thorpe* [1977] to derive optical depths between 0.05 and 0.6, usually between 0.1 and 0.2. Opacities derived from Viking Orbiter limb observations by *Jaquin et al.* [1986] agree with those found by *Pollack et al.* [1977] over the Viking Lander sites but are sometimes lower elsewhere on Mars. Images in which the "hard" planetary limb can be seen indicate that normal optical depths as low as 0.01 sometimes occur. The visibility of surface features places a rough upper limit on the opacity for the images under consideration. Images of interest should have normal optical depths between 0.01 and 1.

Pollack [1982] used Viking Lander sky brightness observations to find ω_0, g, and Q_{ext} as a function of wavelength in visible and near-infrared light. His values of ω_0 are 0.74 and 0.88 at the effective wavelengths of the Viking Orbiter violet and red filters, respectively. Estimates of ω_0 using Viking Orbiter data have a larger difference between the red and the violet filters. *Thorpe* [1978] modeled low-phase observations to find $\omega_0 = 0.5$ (violet) and 0.8–0.85 (red). *Jaquin et al.* [1986] analyzed limb observations to find the same single-scattering albedo (within 0.1) as Thorpe in violet light but $\omega_0 = 0.94$ through the red filter. We expect that $0.5 \leq \omega_0 \leq 0.7$ for the violet filter and $0.8 \leq \omega_0 \leq 0.95$ for the red filter and that the single-scattering albedo in green light will be intermediate between those in violet and red light.

The asymmetry parameter g of Martian dust is known to be positive (forward scattering), but its determination is highly model-dependent [*Zurek*, 1982]. An asymmetry parameter for the red filter of 0.6 was used by *Jaquin et al.* [1986], while *Kattawar and Young* [1977] found that $g = 0.63$ fit their data well at similar wavelengths. The asymmetry factor given by *Pollack et al.* [1979] cannot be directly compared because they did not use a Henyey-Greenstein

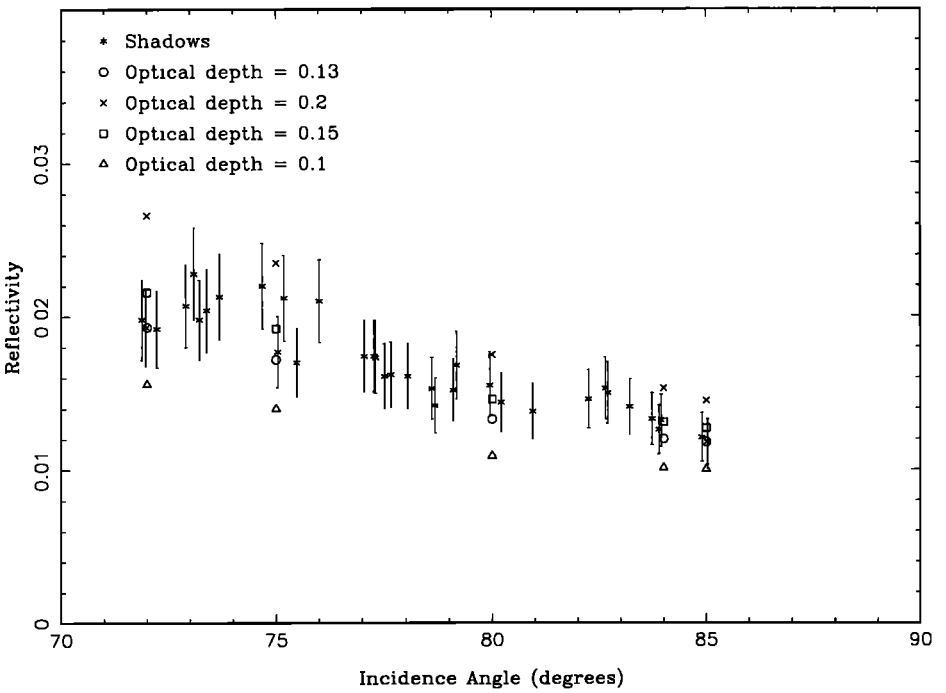

Fig. A1. Viking Orbiter 2 orbit 407 violet (λ_{eff} = 0.45 μ) shadow data with model fits, showing effect of varying optical depth. The vertical scatter in the data is due to the inclusion of unshadowed ground below the resolution of the images, especially at lower incidence angles, so the model was fit to the lower limit of the shadow data. Error bars represent the 13% absolute uncertainty in the VIking Orbiter television calibration [*Klaasen et al.*, 1977].

phase function. *Lumme et al.* [1981] modeled ground-based photometric data to find $g = 0.35 \pm 0.10$ in the V band. *Jaquin et al.* [1986] state that g is between 0.35 and 0.55 through the violet filter but are less confident of their violet results. *Thorpe* [1979, 1981] found that g ranges from 0.0 to 0.6, and we expect that the asymmetry parameter should be in this range.

Ground-based spectrophotometric studies have shown

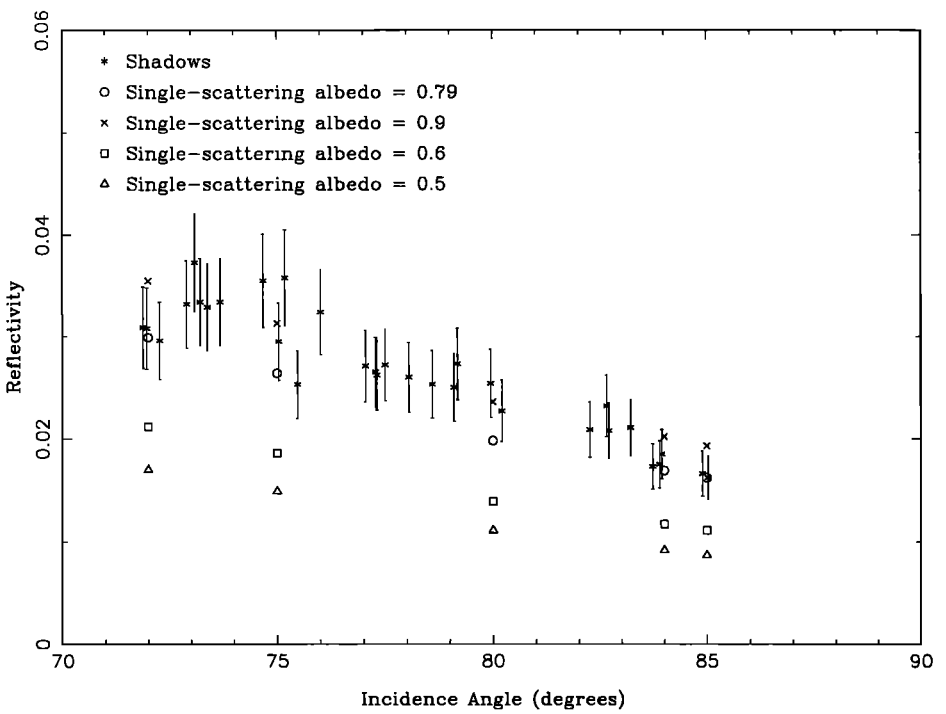

Fig. A2. Viking Orbiter 2 orbit 407 green (λ_{eff} = 0.54 μ) shadow data with model fits, showing effect of varying single-scattering albedo.

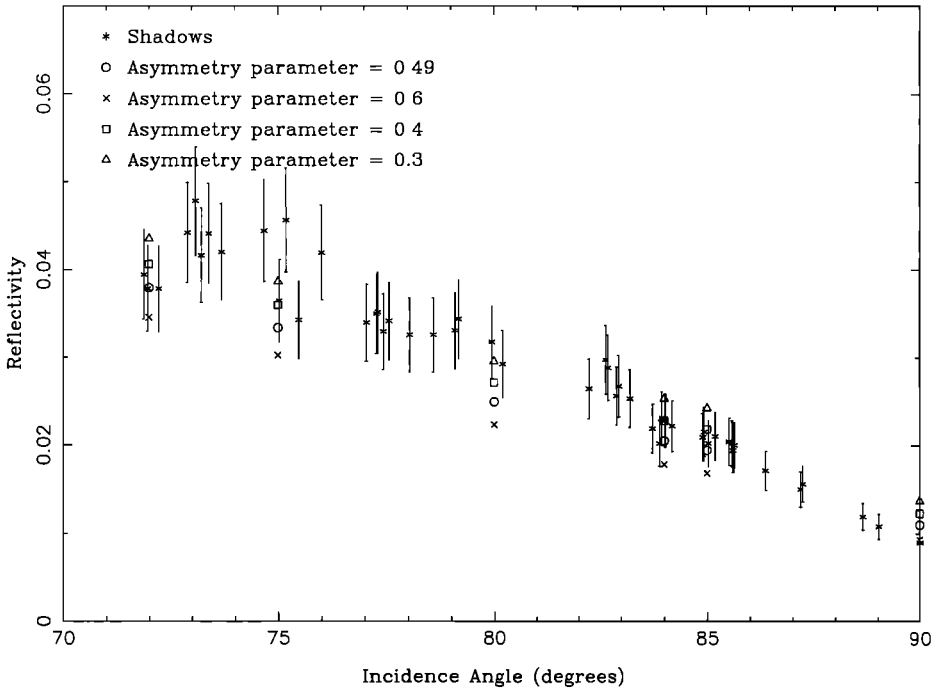

Fig. A3. Viking Orbiter 2 orbit 407 red (λ_{eff} = 0.59 μ) shadow data with model fits, showing effect of varying asymmetry parameter. Uncertainties in the shadow data are larger at high incidence angles because of the greater uncertainty in absolute calibration at low exposure levels.

that spatial variations in Mars' reflectivity are small at blue wavelengths [*McCord and Westphal*, 1971]. Therefore we use r_0 = 0.09 for the violet filter, which has a very similar band pass to the B (blue) filter used by *Lumme et al.* [1981]. Although the spectral reflectivity of the Martian surface in the south polar region has not been measured, telescopic maps of Mars indicate that it has an intermediate albedo. We expect the green and red surface reflectances to be greater than that of Syrtis Major (r_0(green) = 0.11; r_0(red) = 0.14) but less than Arabia's (r_0(green) = 0.18; r_0(red) = 0.28). These reflectances were derived by integration of the spectral geometric albedo data given by *McCord and Westphal* [1971] over the spectral band passes of the Viking Orbiter cameras [K. Klaasen, personal communication, 1987). They were then increased by 10% to agree with the blue band data of *Lumme et al.* [1981] and earlier studies [*McCord and Adams*, 1969]. The surface albedo is assumed to be constant in the atmospheric model. Actual unfrosted ground albedos in the color mosaic vary by about a factor of 2, resulting in errors in atmospheric brightness of the same order as the absolute uncertainty in the calibration of the Viking cameras: 13%. Good shadow data near 75.5° incidence angle were used to subtract the atmospheric component from the observed violet and red brightnesses of nearby plains. The resulting surface reflectances have an *R/V* ratio of 2.8, so r_0(red) = 0.25 is used in the model.

TABLE 2. Atmospheric Dust-Scattering Parameters

Filter	Violet	Green	Red
r_0	0.09	0.18	0.25
ω_0	0.57	0.79	0.85
g	0.31	0.47	0.49
Q_{ext}	2.64	2.71	2.75

A three-color mosaic of Viking Orbiter 2 images of the south polar region was used to evaluate the brightness of the atmosphere in shadows during orbit 407. Only the largest shadows gave consistent results, because of the moderate resolution of the images, and we have chosen minimum brightness levels that are represented by at least 2 pixels to avoid noisy data. The vertical scatter in the shadow data (Figures A1–A3) is partly caused by the inclusion of unshadowed terrain in some of the pixels, especially at lower incidence angles. Variations in surface albedo and roughness may also contribute to the scatter but are not easily modeled. In addition, spatial variations in dust opacity will cause some scatter. We were unable to find good shadows in the mosaic at incidence angles less than 70°. Near the terminator, shadows are longer, and there is less scatter, giving us confidence that the pixel values at high incidence angles are not contaminated by unshadowed ground. With this in mind we have endeavored to construct a model that defines a lower limit to the shadow data.

The best fit of the shadow data with the parameters described above has τ = 0.13 and surface albedos and dust scattering parameters as shown in Table 2. The spectral reflectances used are very similar to the spectral geometric albedo of "intermediate albedo" areas given by *McCord and Westphal* [1971] and to the reflectances of the soils at the Viking Lander 1 site [*Guinness*, 1981] when differences in spectral band pass are taken into account. The effect of varying τ is shown in Figure A1, ω_0 in Figure A2, and g in Figure A3. An image taken through the red filter during the same orbit (that was not included in the mosaic) was used to evaluate the atmospheric reflectance at the terminator. Sev-

eral of the best shadow data points were chosen for modeling (on the basis of their low values in all three colors) near 72°, 80°, 84°, and 85° incidence angle and at the terminator. The observational geometry of each of these points was determined using Supplementary Experiment Data Record (SEDR) data. The model fits the data within the 13% uncertainties except at 80°, where the shadows are evidently contaminated with illuminated ground below the resolution of the images or the dust opacity is greater. Radiometric uncertainties in images exposed to low light levels are generally larger than for brighter scenes, so the discrepancy between the model and the data at the terminator is not considered serious. Variations in emission and azimuth angles across the mosaic have a significant effect on the atmospheric brightness and have been included in the model.

Once the optical depth and other model parameters have been determined in shadows, other points in the image can be modeled. Interpolation between modeled points in the image yields the approximate atmospheric brightness at any point, allowing removal of the atmospheric component of brightness across the entire image or any part of it. The interpolated atmospheric brightness is subtracted from the data value in each pixel, and the result is divided by the incoming and outgoing attenuation to find what the surface reflectivity would be if there were no atmosphere. This technique assumes that dust-scattering properties and surface albedos are invariant across the image and that the shadowed regions are small compared to the dust scale height, so that their presence does not alter the atmospheric brightness. Variations in surface albedo are small in the area modeled, except in the polar frost. The effect of low surface albedos in modeling of atmospheric scattering over the polar cap is discussed in the text. Although there is evidence in the color mosaic of spatial variations in dust opacity, it is not possible to account for such variability in this model. Errors due to interpolation are generally less than 3% (as indicated by model runs at points between those used), while variations in opacity are seen to cause up to 20% variations in atmospheric brightness. Topographic variations in the south polar region are not precisely known, but a 1-km increase in altitude decreases the modeled atmospheric brightness by only 11%. The effect of topographic variations was not included in this model but could be incorporated in the future.

Acknowledgments. Tammy Becker and Larry Soderblom at the U.S. Geological Survey in Flagstaff made helpful suggestions and created the Viking color mosaic that made much of this work possible. We also thank Yuk Yung for allowing us to use his RADIATE program, Mark Allen for his assistance in modifying and implementing it, and Andrew Ingersoll and David Crisp for helpful discussions. Detailed reviews by Alfred McEwen and Peter Thomas are also appreciated. This work was supported by NASA grants NGT-50096 and NAGW-1226. Contribution 4713 of the Division of Geological and Planetary Sciences.

REFERENCES

Arvidson, R. E., Aeolian processes on Mars: Erosive velocities, settling velocities, and yellow clouds, *Geol. Soc. Am. Bull., 83*, 1503–1508, 1972.

Carr, M. H., Periodic climate change on Mars: review of evidence and effects on distribution of volatiles, *Icarus, 50*, 129–139, 1982.

Clark, R. N., and P. G. Lucey, Spectral properties of ice-particulate mixtures and implications for remote sensing, I, Intimate mixtures, *J. Geophys. Res., 89*, 6341–6348, 1984.

Cutts, J. A., Nature and origin of layered deposits of the Martian polar regions, *J. Geophys. Res., 78*, 4231–4249, 1973.

Cutts, J. A., K. R. Blasius, and W. J. Roberts, Evolution of Martian polar landscapes: Interplay of long-term variations in perennial ice cover and dust storm intensity, *J. Geophys. Res., 84*, 2975–2994, 1979.

Greeley, R., R. Leach, B. White, J. Iversen, and J. Pollack, Threshold windspeeds for sand on Mars: Wind tunnel simulations, *Geophys. Res. Lett., 7*, 121–124, 1980.

Guinness, E. A., Spectral properties (0.40 to 0.75 microns) of soils exposed at the Viking 1 landing site, *J. Geophys. Res., 86*, 7983–7992, 1981.

Hargraves, R. B., D. W. Collinson, R. E. Arvidson, and P. M. Cates, Viking Magnetic Properties Experiment: Extended mission results, *J. Geophys. Res., 84*, 8379–8384, 1979.

Hofstadter, M. D., and B. C. Murray, Ice sublimation and rheology: Implications for the Martian polar layered deposits, *Icarus*, in press, 1989.

Howard, A. D., Origin of the stepped topography of the Martian poles, *Icarus, 34*, 581–599, 1978.

Howard, A. D., J. A. Cutts, and K. R. Blasius, Stratigraphic relationships within Martian polar cap deposits, *Icarus, 50*, 161–215, 1982.

Iversen, J. D., and B. R. White, Saltation thresholds on Earth, Mars, and Venus, *Sedimentology, 29*, 111–119, 1982.

James, P. B., G. Briggs, J. Barnes, and A. Spruck, Seasonal recession of Mars' south polar cap as seen by Viking, *J. Geophys. Res., 84*, 2889–2922, 1979.

Jaquin, F., P. Gierasch, and R. Kahn, The vertical structure of limb hazes in the Martian atmosphere, *Icarus, 68*, 422–461, 1986.

Kahn, R., R. Goody, and J. Pollack, The Martian twilight, *J. Geophys. Res., 86*, 5833–5838, 1981.

Kattawar, G. W., and A. T. Young, Planetary isophotes as a clue to aerosol characteristics, *Icarus, 30*, 367–376, 1977.

Kieffer, H. H., Mars south polar spring and summer temperatures: A residual CO_2 frost, *J. Geophys. Res., 84*, 8263–8288, 1979.

Klaasen, K. P., T. E. Thorpe, and L. A. Morabito, Inflight performance of the Viking visual imaging subsystem, *Appl. Opt., 16*, 3158–3170, 1977.

Lumme, K., L. J. Martin, and W. A. Baum, Theoretical interpretation of photometric properties of the Martian surface and atmosphere, *Icarus, 45*, 379–397, 1981.

McCord, T. B., and J. B. Adams, Spectral reflectivity of Mars, *Science, 163*, 1058–1060, 1969.

McCord, T. B., and J. A. Westphal, Mars: Narrow-band photometry, from 0.3 to 2.5 microns, of surface regions during the 1969 apparition, *Astrophys. J., 168*, 141–153, 1971.

Murray, B. C., L. A. Soderblom, J. A. Cutts, R. P. Sharp, D. J. Milton, and R. B. Leighton, Geological framework of the south polar region of Mars, *Icarus, 17*, 328–345, 1972.

Paige, D. A., The annual heat balance of the Martian polar caps from Viking observations, Ph.D. thesis, Calif. Inst. of Technol., Pasadena, 1985.

Paige, D. A., and H. H. Kieffer, The thermal properties of Martian surface materials at high latitudes: Possible evidence for permafrost, *Tech. Rep. 87-01*, pp. 93–95, Lunar and Planet. Inst. Houston, Tex., 1987.

Pike, F. J., Simple to complex craters: The transition on Mars, *NASA Tech. Memo. 80339*, pp. 132–134, 1979.

Plaut, J. J., R. Kahn, E. A. Guinness, and R. E. Arvidson, Accumulation of sedimentary debris in the south polar region of Mars and implications for climate history, *Icarus, 75*, 357–377, 1988.

Pollack, J. B., Properties of dust in the Martian atmosphere and its effect on temperature structure, *Adv. Space Res., 2*, 45–56, 1982.

Pollack, J. B., D. Colburn, R. Kahn, J. Hunter, W. Van Camp, C. E. Carlston, and M. R. Wolf, Properties of aerosols in the Martian atmosphere, as inferred from Viking lander imaging data, *J. Geophys. Res., 82*, 4479–4496, 1977.

Pollack, J. B., D. Colburn, F. M. Flasar, R. Kahn, C. Carlston, and D. Pidek, Properties and effects of dust particles suspended in the Martian atmosphere, *J. Geophys. Res., 84*, 4479–4496, 1979.

Saunders, R. S., T. J. Parker, J. B. Stephens, E. G. Laue, and F. P. Fanale, Transformation of polar ice sublimate residue into Mar-

tian circumpolar sand, *NASA Tech. Memo. 87563*, pp. 300–302, 1985.

Saunders, R. S., F. P. Fanale, T. J. Parker, J. B. Stephens, and S. Sutton, Properties of filamentary sublimation residues from dispersions of clay in ice, *Icarus, 66*, 94–104, 1986.

Squyres, S. W., The evolution of dust deposits in the Martian north polar region, *Icarus, 40*, 244–261, 1979.

Storrs, A. D., F. P. Fanale, R. S. Saunders, and J. B. Stephens, The formation of filamentary sublimate residues (FSR) from mineral grains, *Icarus, 76*, 493–512, 1988.

Tanaka, K. L., and D. H. Scott, Geologic map of the polar regions of Mars, *U.S. Geol. Surv. Misc. Invest. Ser. Map*, I-1802-C, 1987.

Thomas, P., Present wind activity on Mars: Relation to large latitudinally zoned sediment deposits, *J. Geophys. Res., 87*, 9999–10,008, 1982.

Thomas, P. C., and C. Weitz, Dune sand materials and polar layered deposits on Mars, *Icarus, 81*, 185–215, 1989.

Thorpe, T. E., Viking Orbiter photometric observations of the Mars phase function July through November 1976, *J. Geophys. Res., 82*, 4161–4165, 1977.

Thorpe, T. E., Viking Orbiter observations of the Mars opposition effect, *Icarus, 36*, 204–215, 1978.

Thorpe, T. E., A history of Mars atmospheric opacity in the southern hemisphere during the Viking extended mission, *J. Geophys. Res., 84*, 6663–6683, 1979.

Thorpe, T. E., Mars atmospheric opacity effects observed in the northern hemisphere by Viking Orbiter imaging, *J. Geophys. Res., 86*, 11,419–11,429, 1981.

Toon, O. B., J. B. Pollack, W. Ward, J. A. Burns, and K. Bilski, The astronomical theory of climate change on Mars, *Icarus, 44*, 552–607, 1980.

Wechsler, A. E., and P. E. Glaser, Pressure effects on postulated lunar materials, *Icarus, 4*, 335–352, 1965.

Winter, D. F., and J. M. Saari, A particulate thermophysical model of the lunar soil, *Astrophys. J., 156*, 1135–1151, 1969.

Zurek, R. W., Martian great dust storms: An update, *Icarus, 50*, 288–310, 1982.

K. E. Herkenhoff and B. C. Murray, Division of Geological and Planetary Sciences, California Institute of Technology, Pasadena, CA 91125.

(Received September 19, 1988;
revised April 6, 1989;
accepted April 6, 1989.)